



Santalol Isomers Inhibit Transthyretin Amyloidogenesis and Associated Pathologies in *Caenorhabditis elegans*

Amirthalingam Mohankumar^{1,2*}, Duraisamy Kalaiselvi³, Govindhan Thiruppathi², Sivaramkrishnan Muthusaravanan⁴, Subramaniam Vijayakumar⁵, Rahul Suresh⁶, Shinkichi Tawata^{1*} and Palanisamy Sundararaj^{2*}

¹PAK Research Center, University of the Ryukyus, Okinawa, Japan, ²Department of Zoology, Bharathiar University, Coimbatore, India, ³Department of Agricultural Chemistry, Institute of Environmentally Friendly Agriculture, College of Agriculture and Life Science, Chonnam National University, Gwangju, South Korea, ⁴Department of Biotechnology, Mepco Schlenk Engineering College, Sivakasi, India, ⁵Department of Medical Physics, Bharathiar University, Coimbatore, India, ⁶International Research Center of Spectroscopy and Quantum Chemistry—IRC SQC, Siberian Federal University, Krasnoyarsk, Russia

OPEN ACCESS

Edited by:

Zebo Huang,
South China University of Technology,
China

Reviewed by:

Pierfausto Seneci,
University of Milan, Italy
Maria Rosário Almeida,
Universidade do Porto, Portugal

*Correspondence:

Amirthalingam Mohankumar
amkkmohan@gmail.com
Shinkichi Tawata
b986097@agr.u-ryukyu.ac.jp
Palanisamy Sundararaj
sunpalan@gmail.com

Specialty section:

This article was submitted to
Experimental Pharmacology and Drug
Discovery,
a section of the journal
Frontiers in Pharmacology

Received: 20 April 2022

Accepted: 25 May 2022

Published: 16 June 2022

Citation:

Mohankumar A, Kalaiselvi D,
Thiruppathi G, Muthusaravanan S,
Vijayakumar S, Suresh R, Tawata S
and Sundararaj P (2022) Santalol
Isomers Inhibit Transthyretin
Amyloidogenesis and Associated
Pathologies in *Caenorhabditis elegans*.
Front. Pharmacol. 13:924862.
doi: 10.3389/fphar.2022.924862

Transthyretin (TTR) is a homotetrameric protein found in human serum and is implicated in fatal inherited amyloidoses. Destabilization of native TTR conformation resulting from mutation, environmental changes, and aging causes polymerization and amyloid fibril formation. Although several small molecules have been reported to stabilize the native state and inhibit TTR aggregation, prolonged use can cause serious side effects. Therefore, pharmacologically enhancing the degradation of TTR aggregates and kinetically stabilizing the native tetrameric structure with bioactive molecule(s) could be a viable therapeutic strategy to hinder the advancement of TTR amyloidoses. In this context, here we demonstrated α - and β -santalol, natural sesquiterpenes from sandalwood, as a potent TTR aggregation inhibitor and native state stabilizer using combined *in vitro*, *in silico*, and *in vivo* experiments. We found that α - and β -santalol synergize to reduce wild-type (WT) and Val30Met (V30M) mutant TTR aggregates in novel *C. elegans* strains expressing TTR fragments fused with a green fluorescent protein in body wall muscle cells. α - and β -Santalol extend the lifespan and healthspan of *C. elegans* strains carrying TTR_{WT}::EGFP and TTR_{V30M}::EGFP transgene by activating the SKN-1/Nrf2, autophagy, and proteasome. Moreover, α - and β -santalol directly interacted with TTR and reduced the flexibility of the thyroxine-binding cavity and homotetramer interface, which in turn increases stability and prevents the dissociation of the TTR tetramer. These data indicate that α - and β -santalol are the strong natural therapeutic intervention against TTR-associated amyloid diseases.

Keywords: transthyretin, familial amyloid polyneuropathy, santalol isomers, synergism, *Caenorhabditis elegans*, tetramer stabilizer

INTRODUCTION

Hereditary amyloidogenic transthyretin (ATTR) amyloidosis with polyneuropathy, commonly known as transthyretin-type familial amyloid polyneuropathy (FAP), is a sparse condition mostly found in Japan, France, Portugal, Sweden, Spain, and descendants of these regions (Coelho et al., 2013). FAP is a life-limiting, autosomal dominant, severe systemic disorder with

predominant somatic and autonomic peripheral nervous system involvement caused by a mutation in the transthyretin gene (*TTR*) (Benson et al., 2020). FAP is characterized by the extracellular deposition of amyloid fibril containing insoluble mutant *TTR* variants. Amyloid fibril deposition can be observed in autonomic and peripheral nerves, heart, intestine, lungs, and carpal tunnel of affected individuals. Familial amyloid cardiomyopathy (FAC) and senile systemic amyloidosis (SSA) are also caused by the misfolding and subsequent aggregation of mutant and wild-type *TTR*, respectively. Hereditary amyloidosis can be of the wild type (ATTRwt) or the mutated form (ATTRm). ATTRwt is the most common age-related type of amyloid disease, and ATTRm occurs due to various point mutations (Pinney et al., 2013). Over 140 different amyloidogenic *TTR* variants have been reported (Rowczenio et al., 2014). *TTR* is a 55 kDa homotetramer consisting of four identical 14 kDa monomers with 127 amino-acid residues each and is rich in β -sheets with four binding sites; two for retinol (vitamin A)-retinol-binding protein (RBP) complex and two for thyroxine (T_4). *TTR* transports T_4 and the retinol-RBP complex to the brain and various body parts (Hörnberg et al., 2000). Two funnel-shaped T_4 binding pockets are located at the center of the tetramer, which contributes to the stability of the *TTR* by binding with T_4 between two dimers. Tetramer dissociation is the rate-limiting step for *TTR* amyloid fibril formation. Accordingly, point mutations destabilize the native tetrameric *TTR* and thus increase amyloidogenesis (Hammarström et al., 2002). Therefore, stabilizing *TTR* tetramer through pharmacological interventions is a promising strategy for treating *TTR* amyloidoses.

For many years, heart or heart-liver combined transplantation and prophylactic pacemaker implantation have been the only palliative treatments for *TTR* amyloidosis (Holmgren et al., 1991). Recently, it was shown that several bioactive phytochemicals and small molecules could stall *TTR* amyloidogenesis. These molecules are known to bind strongly to the unoccupied T_4 -binding sites within *TTR* and kinetically stabilize the native quaternary structure, which limits the tetramer destabilization and aggregate formation (Adams et al., 2019; Yokoyama and Mizuguchi, 2020). Mounting clinical and preclinical evidence indicated that tafamidis and diflunisal reduced the progression of early- and late-onset ATTRwt and Val30Met (ATTR_{V30M}) amyloidoses and diseases associated with other *TTR* variants (Bulawa et al., 2012; Berk et al., 2013). Sant'Anna and others found that tolcapone, an FDA-approved molecule for Parkinson's disease, inhibits *TTR* aggregation and toxicity, binds to *TTR* in human plasma, and stabilizes the tetramer dissociation in mice and humans (Sant'Anna et al., 2016). Several natural compounds have been shown to prevent the early stage of *TTR* tetramer dissociation and inhibit specific *TTR* fibril formation (Ciccione et al., 2020; Yokoyama and Mizuguchi, 2020; Matsushita et al., 2021). These observations clearly indicated that the pharmacological enhancement of the breakdown of *TTR* aggregates and kinetic stabilization of the native tetrameric structure of *TTR* with bioactive molecules could be a viable therapeutic strategy to hinder the advancement of these diseases. Santalol isomers (α - and β -santalol), the active ingredients in *Santalum album* L.

essential oil, seem promising in this endeavor. Our previous study found that santalol isomers offer stress-resilience, extend healthy longevity, and retard age-related functional deficits in *C. elegans* (Mohankumar et al., 2018; Mohankumar et al., 2019b). Importantly, santalol isomers reduced the protein aggregates strongly associated with pathologies of Alzheimer's, Parkinson's, and Huntington's diseases by activating multiple cellular signaling pathways (Mohankumar et al., 2018; Mohankumar et al., 2020). Here, we identify santalol isomers as a potential inhibitor of *TTR* amyloidogenesis. We have shown that α - and β -santalol act synergistically to reduce the aggregation and toxicity of wild-type and V30M mutant *TTR* and to alleviate other *TTR*-associated pathologies by selectively activating SKN-1/Nrf2, autophagy, and proteasome more effectively than the orally active *TTR* inhibitor tolcapone. Moreover, α - and β -santalol binds to the T_4 -binding site and stabilizes the wild-type and V30M mutant *TTR*, thereby preventing the tetramer dissociation.

MATERIALS AND METHODS

Materials

α - and β -Santalol were purified from sandalwood (*Santalum album* L.) oil as described (Mohankumar et al., 2018). Nematode and bacterial growth media and their components, antibiotics, sodium hydroxide (NaOH), household bleach (NaClO), sodium azide (NaN₃), and dimethyl sulfoxide (DMSO) were purchased from HiMedia Laboratories Pvt. Ltd. (Mumbai, India). Tolcapone, chloroquine, Epigallocatechin gallate (EGCG), isopropyl β -D-1-thiogalactopyranoside (IPTG), 5-fluoro-2'-deoxyuridine (FUdR), 2',7'-dichlorodihydrofluorescein diacetate (H₂DCF-DA), prealbumin from human plasma, and MG-132 were obtained from Sigma Aldrich (St. Louis, MO, United States).

C. elegans Strains, Genetics, and Handling

C. elegans were cultured on standard nematode growth media (NGM) agar plates carrying *E. coli* OP50 and maintained at 20°C using the standard techniques (Brenner, 1974). The wild-type (N2), *hlh-30[tm1978]*, and *bec-1[ok700]* strains were obtained from the *Caenorhabditis* Genetics Centre (CGC, University of Minnesota, MN, United States). The novel strains expressing several type of *TTR* fragments fused with GFP in body wall muscle cells *viz.*, *zyeEx1069[pCKX3307(unc-54p::nsTTR_{WT}::EGFP)]*, *zyeEx1070[pCKX3311(unc-54p::nsTTR₁₋₈₀::EGFP)]*, *zyeEx1073[pCKX3303(unc-54p::nsTTR₈₁₋₁₂₇::EGFP)]*, *zyeEX1076[pCKX3316(unc-54p::nsEGFP)]*, *zyeEx1078[pCKX3309(unc-54p::nsTTR_{V30M}::EGFP)]*, and *zyeEx1082[pCKX3313(unc-54p::nsTTR₄₉₋₁₂₇::EGFP)]* were gifted by Professor Kunitoshi Yamanaka (Kumamoto University, Japan) (Tsuda et al., 2018). Synchronized culture of worms were obtained by alkaline hypochlorite treatment of gravid adult worms as described previously (Stiernagle, 2006).

Lifespan Analysis

Lifespan was measured at 20°C as previously described (Mohankumar et al., 2020). In brief, synchronized L1 stage

worms (10–15 worms per plate for a total of 100–120 individuals per experiment) were raised on plates supplemented with santalol isomers and tolcapone. Worms were scored as live or dead, and surviving nematodes were transferred to fresh plates every day during the reproduction period and 4–5 days thereafter. Animals were censored from the analysis if they suffered from internal hatching, desiccated on the edge of the plate, ruptured, mechanical death, or lost. Death was confirmed and scored based on the failure to respond to mild contact with a metal worm picker and loss of pharynx movement.

Phenotype Assay

To measure the body bends, control and santalol isomers treated worms were gently washed off from the plates and released on the agar plates to crawl for 5 min at 20°C. Individual worms (40 worms per experiment) were transferred to 24-well plates containing 1 ml M9 buffer. After 1 min recovery time, the number of body bends, the reciprocating motion of bends at the mid-body, were scored for 30 s. Mechanosensory neuronal aberrations were measured in the soft-touch sensitivity assay (Pan et al., 2011). On day 5 and day 10 of adulthood, 20–25 randomly selected individuals/experiments were subjected to touch response by counting the number of positive responses to five alternating touches at the posterior and anterior ends of each worm using eyelash (10 total touches/worm). For reproduction assay, worms treated with and without santalol isomers (10 worms per experiment) were individually shifted to fresh NGM plates each day until their reproduction period becomes ceased. The resulting progeny was allowed to develop at 20°C and counted at their adulthood stage. The growth of the worms was measured by body length, which was determined by measuring the flat surface area of control and treated animals (50 worms per experiment) using an image analyzer (Optika, Italy) (Devagi et al., 2018; Mohankumar et al., 2019a). Chemotaxis and food sensing behavior assays were performed as described. For detailed procedures, see the supplementary material.

Visualization of TTR Aggregation

TTR aggregation was measured by using the transgenic lines expressing several types of TTR::EGFP in body wall muscle cells. Synchronized worms (L1 stage; 10–15 individuals per experiment) were grown on NGM plates with and without santalol isomers. On day 2 and day 6 of adulthood, the worms were collected, washed with M9 buffer, and mounted on glass slides for fluorescent microscopy (BX41, Olympus, Japan). Worms were anesthetized using NaN₃ at a final concentration of 25 mM. Fluorescence images were obtained, and the visible TTR::EGFP aggregates were counted. The TTR::EGFP aggregates are spherical-shaped discrete structures, and their boundaries are clearly differentiated from nearby fluorescent signals (Tsuda et al., 2018). At least three independent biological trials were performed at similar conditions with appropriate replicates, as indicated.

Measurement of Intracellular ROS Levels

Intracellular ROS levels in *C. elegans* were measured using the molecular probe H₂DCF-DA. The worms were maintained and

treated as described in the lifespan assay. After treatment, the worms were washed off from the plates with PBST buffer (PBS + 1% Tween 20) and pelleted by centrifugation. The worms were quickly frozen in liquid nitrogen and immediately sonicated for 5 min to disrupt the outer cuticle. The homogenized samples were then transferred to 96-well plates and incubated with 50 μ M H₂DCF-DA solution for 30 min in the dark at 20°C. Fluorescence intensity was measured using a microplate reader at an excitation/emission wavelength of 490/530 nm.

RNA Interferences

The regular feeding RNAi method was performed to inactivate specified genes, as previously described (Timmons et al., 2001). Individual colonies of *E. coli* strain HT115(DE3) transformed with either the RNAi-encoding plasmid (test) or the empty pL4440 vector (control) were grown in LB media containing 100 μ g ml⁻¹ ampicillin for 12 h at 37°C. Bacteria were concentrated fivefold and seeded onto NGM plates containing 100 μ g ml⁻¹ ampicillin and 1 mM IPTG, hood-dried and cultured for 12 h to induce the expression of dsRNA. Synchronized L1 stage worms were transferred to RNAi plates and raised until the young adult stage for efficient knockdowns.

Quantitative Real-Time PCR for Gene Expression

The worms were frozen in liquid nitrogen, thawed on ice, and homogenized at 4°C. Total RNA was extracted using TRIzol reagents (Invitrogen) (He, 2011) and was reverse transcribed into cDNA using a RevertAid First-strand cDNA synthesis kit (Thermo Scientific™) according to the manufacturer's protocol. Quantitative real-time PCR was performed with SYBR Green master mix, and relative gene expression was analyzed using a comparative C_t ($\Delta\Delta$ C_t) method. The housekeeping gene *act-1* was chosen as the reference gene.

Molecular Dynamics Simulation

The molecular docking was implemented in AutoDock Vina (v.1.1.2) to identify the binding affinity of ligands α - and β -santalol towards the TTR_{WT} (PDB ID: 4D7B) and TTR_{V30M} (PDB ID: 4TL4) (Trott and Olson, 2009). The molecular dynamics simulation of apoproteins and ligand-bound complexes was performed in the GROMACS v2016.4 package using the CHARMM36 all-atom force field at neutral pH and 310 K. The binding energy components ΔE_{vdw} , ΔE_{ele} , ΔG_{pb} , ΔG_{sa} , and ΔG_{bind} were calculated by the molecular mechanics/Poisson-Boltzmann surface area approach. A detailed experimental procedure is given in the electronic supplementary material.

Statistical Analyses

The lifespan of worms was graphed as Kaplan-Meier survival curves with MedCalc statistical tool (MedCalc 14.8.1, Ostend, Belgium) and analyzed using the log-rank (Mantel-Cox) test. The differences between control and santalol isomers-treated groups were statistically compared by one-way analysis of variance (ANOVA; 95% confidence interval) followed by Bonferroni's post hoc test (SPSS 17, IBM Corporation, NY, United States)

and presented as mean \pm standard deviation (SD)/standard error of the mean (SEM) of at least three separate experiments, unless otherwise noted. The probability level of $p < 0.05$ was considered to be statistically significant between the means.

RESULTS AND DISCUSSION

α - and β -Santalol Inhibit TTR Aggregation and Stabilize the TTR Dimer-Dimer Interface

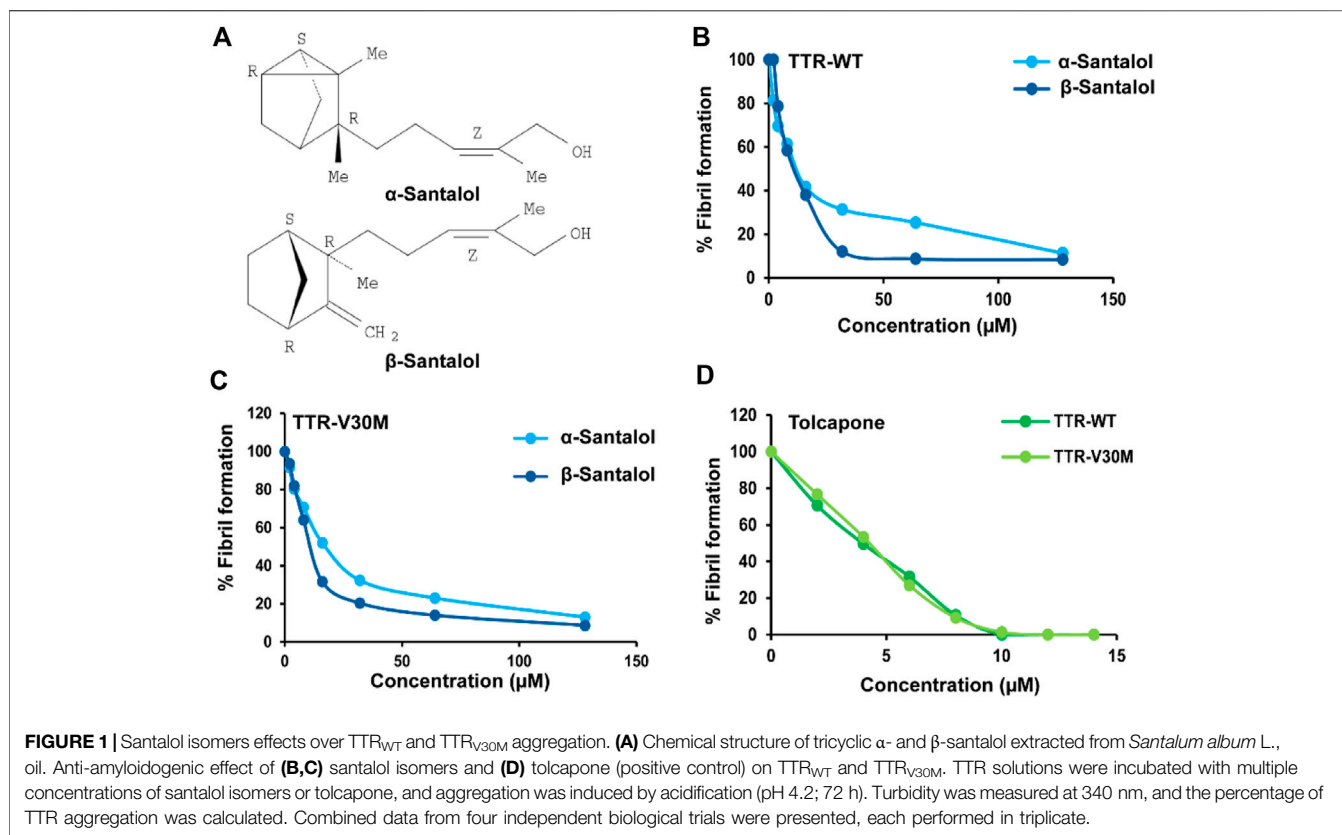
We first tested the TTR inhibitory potential of santalol isomers (Figure 1A) under *in vitro* conditions at low pH (4.2). This acidic pH induces TTR fibril formation, thus increasing sample turbidity and light scattering. The results showed that α - and β -santalol were effective at inhibiting both TTR_{WT} (EC₅₀: 36.7 \pm 1.2 μ M; 31.1 \pm 2.4 μ M) and TTR_{V30M} aggregation (EC₅₀: 44.3 \pm 3.5 μ M; 34.5 \pm 2.8 μ M) under acidic denaturation conditions (pH 4.2, 72 h) (Figures 1 B,C). Under similar conditions, the positive control tolcapone more effectively prevents the aggregation of TTR_{WT} and TTR_{V30M} with EC₅₀ values of 4.6 \pm 0.5 and 4.8 \pm 0.7 μ M, respectively (Figure 1D, Supplementary Table S1), as measured by light scattering. Next, we addressed whether the anti-aggregational activity of santalol isomers is mediated through tetramer stabilization. Tetramer dissociation is believed to be the rate-limiting step for FAP, and stabilization of the native TTR tetramer through pharmacological interventions is a promising strategy for treating TTR amyloidosis. Several small molecules, nonsteroidal anti-inflammatory drugs, and bioactive phytochemicals have recently been demonstrated to delay or even halt TTR aggregation by kinetically stabilizing the native tetrameric form of TTR by binding to the T₄-binding sites, thus increasing the energy barrier of tetramer dissociation (Klabunde et al., 2000; Johnson et al., 2005; Sant'Anna et al., 2016; Tsuda et al., 2018). However, some details of this mechanism remain to be explored. The pharmacological stabilization of TTR tetramer with tafamidis has been approved by the European Medicines Agency to treat early-stage FAP and is currently available in Japan and Europe (Bulawa et al., 2012). Unfortunately, tafamidis fails to treat advanced TTR amyloidosis and has some adverse effects (Lozeron et al., 2013; Huber et al., 2019). With this understanding, we performed *in vitro* TTR stabilization assay to address whether the TTR inhibitory potential of santalol isomers was mediated through tetramer stabilization. TTR dissociation was induced by urea and tracked by monitoring the changes in Trp fluorescence (Hurshman et al., 2004). The results showed that α - and β -santalol prevents urea-induced TTR_{WT} and TTR_{V30M} denaturation and allows a large amount of TTR to remain in its native state. It was found that the TTR stabilizing efficacy of santalol isomers was found to be dose-dependent. α - and β -Santalol exerted a strong stabilizing effect on TTR_{WT} and TTR_{V30M} at 64 μ M and allowed less than 30% of TTR in the unfolded state upon incubation in 8 M urea, which indicates a strong impact on TTR kinetic stability. In contrast, the percentage of folded TTR was reduced to 61.6% (TTR_{WT}) and 75.9% (TTR_{V30M}) in the absence of santalol isomers or tolcapone. In

the positive control (tolcapone, 8 μ M), however, more than 90% of TTR remains in the native state (Supplementary Figure S1).

To further strengthen the *in vitro* results, we, therefore, performed molecular dynamics simulations to identify the possible interaction of santalol isomers with T₄ binding sites. The crystal structures of tolcapone bound to TTR variants (TTR_{WT} and V122I) were solved previously (Sant'Anna et al., 2016). X-ray crystallography studies have shown that tolcapone buried deep within the T₄ binding cavity and its 4-methylphenyl ring forms hydrophobic contacts with residues ALA108, LEU110, SER117, and THR119. Additionally, a hydrogen bonding was also observed between tolcapone's central carbonyl group and the hydroxyl side chain of THR119. However, the atomic insights on the binding of santalol isomers to TTR remain unknown. Therefore, the crystal structures of TTR_{WT} and TTR_{V30M} were subjected to 50 ns MD simulation at physiological conditions in a neutral TIP3P aqueous box employing the CHARMM36 all-atom force field. The final stable apo-protein structures at 50 ns were extracted and used as receptors for molecular docking analysis. The active site of the TTR variants was predicted using CASTp (Tian et al., 2018), and ligands α - and β -santalol were docked to the predicted binding site. To study subsequent conformational changes on TTR_{WT} and TTR_{V30M} complexes upon ligand binding, the best poses selected from docking analysis were subjected to further 50 ns MD simulation at physiological conditions in a neutral TIP3P aqueous box employing the CHARMM36 all-atom force field. For comparison purposes, the apo forms of TTR_{WT} and TTR_{V30M} were also simulated. The apo TTR_{WT} and TTR_{V30M} reached an equilibrium around 20 ns. Thus, we decided the simulation duration of 50 ns was sufficient to analyze the conformational changes and intermolecular interactions.

α -Santalol showed a binding affinity of -5.9 kcal/mol towards TTR_{WT}; it is observed that residues LEU110 (2.84 Å), SER117 (2.49 Å), and THR118 (3.31 Å) were involved in hydrogen bonding, whereas residues ALA108 (3.80 Å) and LEU110 (3.84 Å) were hydrophobic contacts. β -Santalol showed a binding affinity of -5.5 kcal/mol towards the TTR_{WT} and formed five hydrogen bonds with residues ALA108 (2.36 Å), LEU110 (2.85 Å), SER117 (2.48 Å), THR118 (3.29 Å), whereas the residues THR119 (3.34 Å), and LYS15 (3.53 Å), LEU17 (3.71 Å), ALA108 (3.60 Å), and LEU110 (3.42 Å) were hydrophobic contacts. The binding affinity of α - and β -santalol towards the TTR_{V30M} binding site were -5.4 and -6.1 kcal/mol, respectively. α -Santalol interacts with the residue THR119 (2.71 Å) through hydrogen bonding and has strong hydrophobic interactions with residues VAL93 (3.67 Å), PHE95 (3.58 Å), PHE95 (3.70 Å), THR118 (3.74 Å), ALA120 (3.62 Å), and VAL122 (3.48 Å). β -Santalol forms two hydrogen bonds with residue THR96 (2.16 Å, 2.18 Å), and residues PHE95 (3.40 Å), THR105 (3.59 Å), THR118 (3.65 Å), and ALA120 (3.31 Å) were hydrophobic contacts. Hydrogen bonding and hydrophobic contacts play a crucial role in forming and stabilizing energetically-favored protein-ligand complexes (Patil et al., 2010; Sivaramakrishnan et al., 2019). The post docking analysis suggests that the santalol isomers possess a higher binding affinity towards TTR_{WT} than TTR_{V30M}.

TTR_{WT} and TTR_{V30M} apo forms showed RMSD values of 0.2 and 0.15 Å, respectively. RMSD curves of both apo forms and ligand-bound complexes were less than 0.3 Å during the 20 ns simulation; even the most flexible complexes cannot touch 0.3 Å.



This implies that all the structures reached the equilibrium state during the simulation. β -Santalol has a larger RMSD for the TTR_{V30M} than that of TTR_{WT}. As shown in **Figures 2A,B**, β -santalol bounded TTR variants obtained high stability after 20 ns, whereas α -santalol bounded complexes exhibited noticeable fluctuations. In the case of TTR_{V30M}, RMSD for α -santalol bounded complexes increases throughout the simulation, while for TTR_{WT}, a spike in RMSD values was initially noted, decreased for a short duration, and then attained equilibrium at 40 ns. As shown in **Figures 2A,B**, β -santalol bounded TTR variants exhibited enhanced conformational stability than the α -santalol bounded TTR variants during the 20–50 ns.

The RMSF analysis was performed to estimate the fluctuation of each residue on TTR variants upon ligand binding. As presented in **Figures 2C,D**, the RMSF plot shows a variation in the degree of flexibility among residues in both apo form and ligand bounded TTR complexes, indicating that the loop regions showed more flexibility than β -sheets. Moreover, the TTR with point mutation V30M results in a higher degree of flexibility than the wild-type, especially in the active site and homotetramer interface regions. β -Santalol is bound to both TTR_{WT} and TTR_{V30M} and reduces the flexibility at the residue level. In both TTR_{WT} and TTR_{V30M} apo forms, a large magnitude fluctuation was observed in the homotetramer interface until the binding of β -santalol. The RMSD and RMSF analysis of MD trajectories suggest binding of β -santalol reduces the flexibility of the homotetramer interface and provides enhanced conformational stability to the TTR variants.

To evaluate the energetics of binding in a more reliable and elaborate way, the energy components ΔE_{vdw} , ΔE_{ele} , ΔG_{pb} , ΔG_{sa} , and ΔG_{bind} were calculated for ligand-bound complexes by the molecular mechanics/Poisson-Boltzmann surface area approach. As shown in **Table 1**, the van der Waals energy (ΔE_{vdw}) of the complexes made the most contribution to the total binding free energy; a similar result was previously observed (Dong et al., 2016). It is clear that both santalol isomers form energetically-favored complexes with TTR variants; however, ΔG_{bind} values suggest that β -santalol has slightly stronger binding towards TTR_{WT} and TTR_{V30M}. These results are highly consistent with molecular docking analysis and MD simulations. From these observations, it was concluded that the santalol isomers interact with TTR variants and reduce the flexibility of the T₄ binding cavity and the homotetramer interface, which in turn confers conformational stability for TTR variants and prevents the dissociation of the tetramer and subsequent self-assembly into toxic oligomers and aggregates.

α - and β -Santalol Synergize to Reduce Wild-Type and Val30Met Mutant TTR Aggregates *In Vivo*

To further examine the effect of santalol isomers on the formation of TTR aggregates *in vivo*, novel transgenic strains expressing several types of fragments and full-length TTR was used. In ATTR amyloidosis, amyloid deposits in tissues consist of full-length TTR and C-terminal TTR fragments. C-terminal

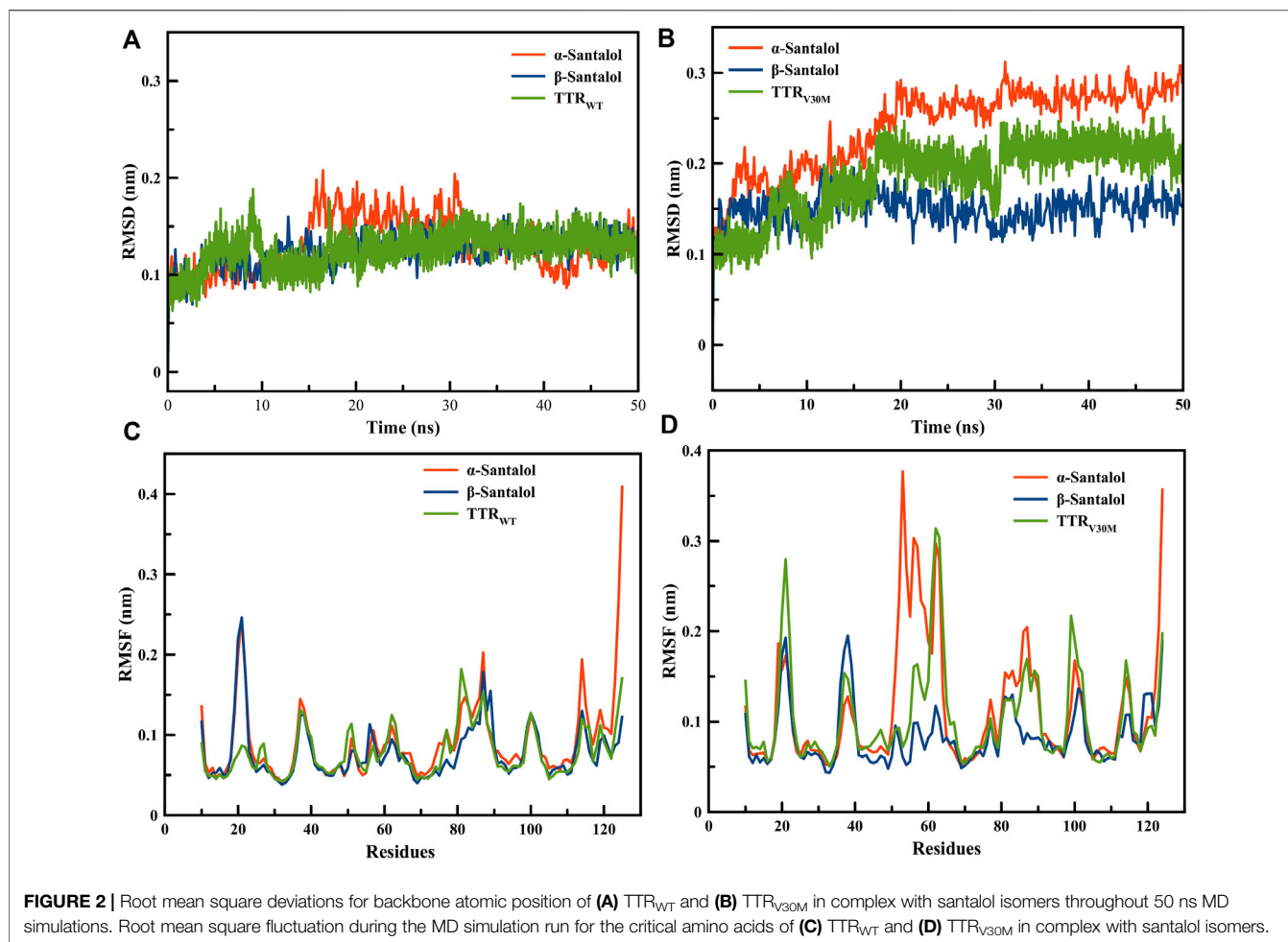


FIGURE 2 | Root mean square deviations for backbone atomic position of (A) TTR_{WT} and (B) TTR_{V30M} in complex with santalol isomers throughout 50 ns MD simulations. Root mean square fluctuation during the MD simulation run for the critical amino acids of (C) TTR_{WT} and (D) TTR_{V30M} in complex with santalol isomers.

TABLE 1 | ΔE_{vdw} , ΔE_{ele} , ΔG_{pb} , and ΔG_{sa} were calculated by the molecular mechanics/Poisson-Boltzmann surface area approach for TTR_{WT} and TTR_{V30M} proteins in complex with santalol isomers along with the corresponding binding free energies.

Complexes	$\Delta E/(\text{kcal mol}^{-1})$				
	ΔE_{vdw}	ΔE_{ele}	ΔG_{pb}	ΔG_{sa}	ΔG_{bind}
α -Santalol_TTR _{WT}	-43.231	-1.782	20.907	-6.164	-30.270
β -Santalol_TTR _{WT}	-48.082	-0.892	14.984	-7.034	-41.024
α -Santalol_TTR _{V30M}	-37.662	-2.200	27.893	-5.639	-17.608
β -Santalol_TTR _{V30M}	-32.972	-0.906	15.302	-4.889	-23.465

fragments of TTR play an important role in aggregate formation *in vitro* as well as *in vivo* (Saelices et al., 2015; Tsuda et al., 2018). Therefore, to investigate the inhibitory effect of santalol isomers against TTR aggregation *in vivo*, *C. elegans* models expressing full-length and C-terminal TTR fragments fused with an enhanced green fluorescent protein (EGFP) in body wall muscle cells *viz.*, TTR_{WT}::EGFP (the full-length wild-type TTR), TTR_{V30M}::EGFP (the full-length TTR but containing V30M mutation), TTR₁₋₈₀::EGFP (the 1–80 residue fragment),

TTR₈₁₋₁₂₇::EGFP (the 81–127 residues fragment), TTR₄₉₋₁₂₇::EGFP (the 49–127 residue fragment), and EGFP alone (as control) were used (Tsuda et al., 2018). TTR_{WT} and TTR_{V30M} are the most common TTR variants, TTR₈₁₋₁₂₇ contains two strong amyloidogenic β -strands—F and H, and TTR₄₉₋₁₂₇ was previously identified in patients with ATTR amyloidosis (Bergström et al., 2005). Moreover, the morphological and structural heterogeneity of the TTR fibrils determines the degree of deposition and reflects the fundamental differences in the pathogenesis of TTR-associated amyloidosis. As a result, we found that worms bearing EGFP alone and TTR₁₋₈₀::EGFP displayed a diffuse localization pattern throughout the body wall muscle cells. TTR_{WT}::EGFP and TTR_{V30M}::EGFP worms gradually developed aggregates with age, and TTR₄₉₋₁₂₇::EGFP and TTR₈₁₋₁₂₇::EGFP worms had spherical shaped discrete aggregates (Figure 3; Table 2; Supplementary Figure S2).

In this study, tolcapone was used as a positive control and is an orally active and reversible inhibitor of catechol-O-methyltransferase (COMT; EC 2.1.1.6), which is approved in Europe and the United States for the treatment of Parkinson’s disease. It has been shown to prevent the onset of TTR misfolding and TTR-induced toxicity by specifically binding and stabilizing the native tetrameric structure of TTR more effectively than

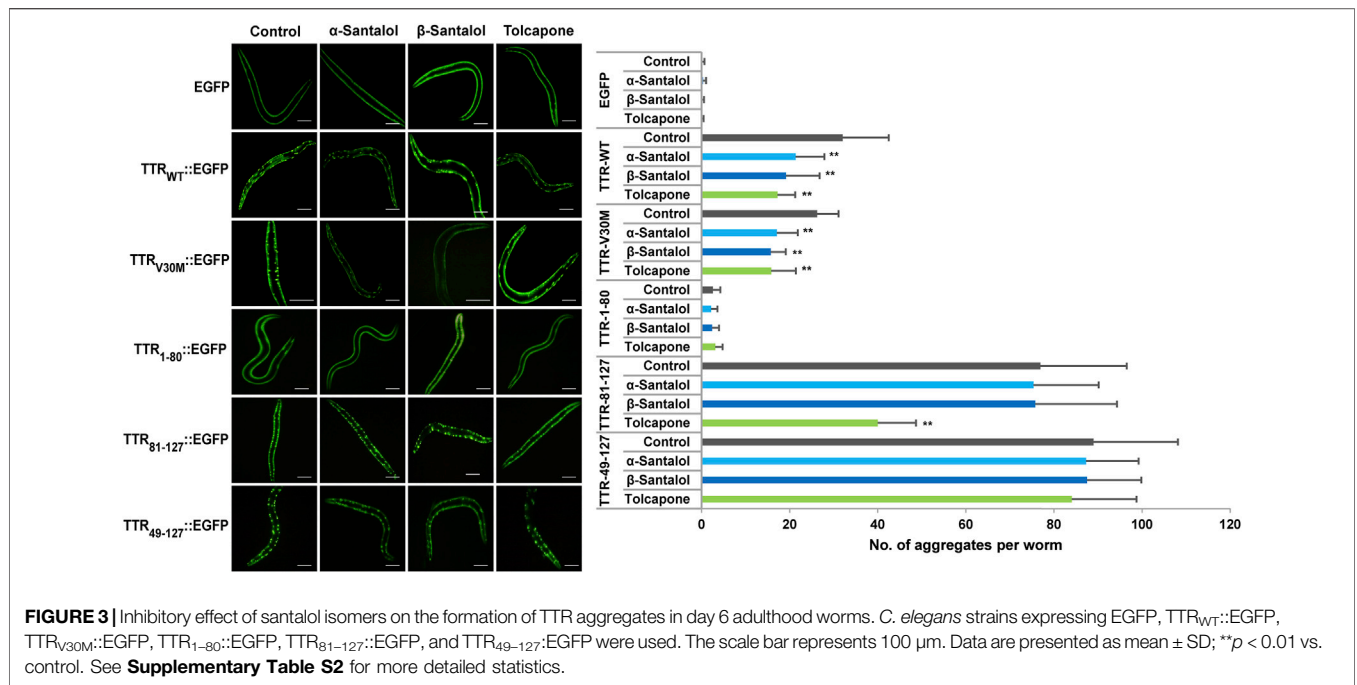


TABLE 2 | Synergistic effect of santalol isomers on the aggregation of different TTR::EGFP aggregates.

Genotype	Treatment (α+β-santalol)	No. of TTR aggregates per worm (n = 40)			
		Day 2		Day 6	
		No. of aggregates ±SD	% Change	No. of aggregates ±SD	% Change
TTR _{WT} ::EGFP	Control	7.73 ± 3.62		32.03 ± 10.44	
	Tolcapone	5.33 ± 3.78 ns	(-) 31.03	17.23 ± 4.07**	(-) 46.20
	4 + 4 μM	7.83 ± 3.92 ns	(+) 1.29	31.47 ± 7.84*	(-) 1.77
	4 + 8 μM	7.67 ± 4.33 ns	(-) 0.86	25.43 ± 8.92 ns	(-) 20.60
	4 + 16 μM	7.17 ± 3.53 ns	(-) 7.33	28.40 ± 10.75 ns	(-) 11.34
	8 + 4 μM	7.83 ± 4.94 ns	(+) 1.29	31.91 ± 6.08 ns	(-) 0.21
	8 + 8 μM	7.63 ± 5.07 ns	(-) 1.29	31.30 ± 7.80**	(-) 2.29
	8 + 16 μM	7.20 ± 3.66 ns	(-) 6.90	24.33 ± 9.89**	(-) 24.04
	16 + 4 μM	7.83 ± 4.40 ns	(+) 1.29	23.00 ± 5.58**	(-) 28.20
	16 + 8 μM	4.80 ± 2.96 ns	(-) 37.93	11.87 ± 5.12**	(-) 62.96
	16 + 16 μM	7.23 ± 4.08 ns	(-) 6.47	22.93 ± 5.00**	(-) 28.41
	32 + 4 μM	7.20 ± 3.68 ns	(-) 6.90	22.03 ± 5.36**	(-) 31.22
	32 + 8 μM	7.07 ± 2.80 ns	(-) 8.62	21.40 ± 4.82**	(-) 33.19
	32 + 16 μM	6.47 ± 4.25 ns	(-) 16.38	17.63 ± 5.35**	(-) 44.95
TTR _{V30M} ::EGFP	Control	8.13 ± 4.30		26.23 ± 4.88	
	Tolcapone	6.17 ± 2.76 ns	(-) 24.18	15.83 ± 5.56**	(-) 39.64
	4 + 4 μM	8.30 ± 3.64 ns	(+) 2.05	27.07 ± 6.64 ns	(+) 3.18
	4 + 8 μM	8.40 ± 4.45 ns	(+) 3.28	25.07 ± 8.91 ns	(-) 4.45
	4 + 16 μM	8.00 ± 3.93 ns	(-) 1.64	24.10 ± 7.55 ns	(-) 8.13
	8 + 4 μM	7.77 ± 3.56 ns	(-) 4.51	21.10 ± 7.91 ns	(-) 19.57
	8 + 8 μM	7.60 ± 3.41 ns	(-) 6.56	22.57 ± 7.61 ns	(-) 13.98
	8 + 16 μM	7.77 ± 3.46 ns	(-) 4.51	21.10 ± 9.60 ns	(-) 19.57
	16 + 4 μM	7.30 ± 3.41 ns	(-) 10.25	20.73 ± 6.73 ns	(-) 20.97
	16 + 8 μM	5.17 ± 2.78 ns	(-) 36.48	12.47 ± 4.28**	(-) 52.48
	16 + 16 μM	7.63 ± 4.51 ns	(-) 6.15	21.23 ± 6.31 ns	(-) 19.06
	32 + 4 μM	7.17 ± 3.09 ns	(-) 11.89	20.13 ± 6.32 ns	(-) 23.25
	32 + 8 μM	7.63 ± 4.22 ns	(-) 6.15	20.60 ± 6.41 ns	(-) 21.47
	32 + 16 μM	7.17 ± 3.74 ns	(-) 11.89	18.97 ± 6.43**	(-) 27.70

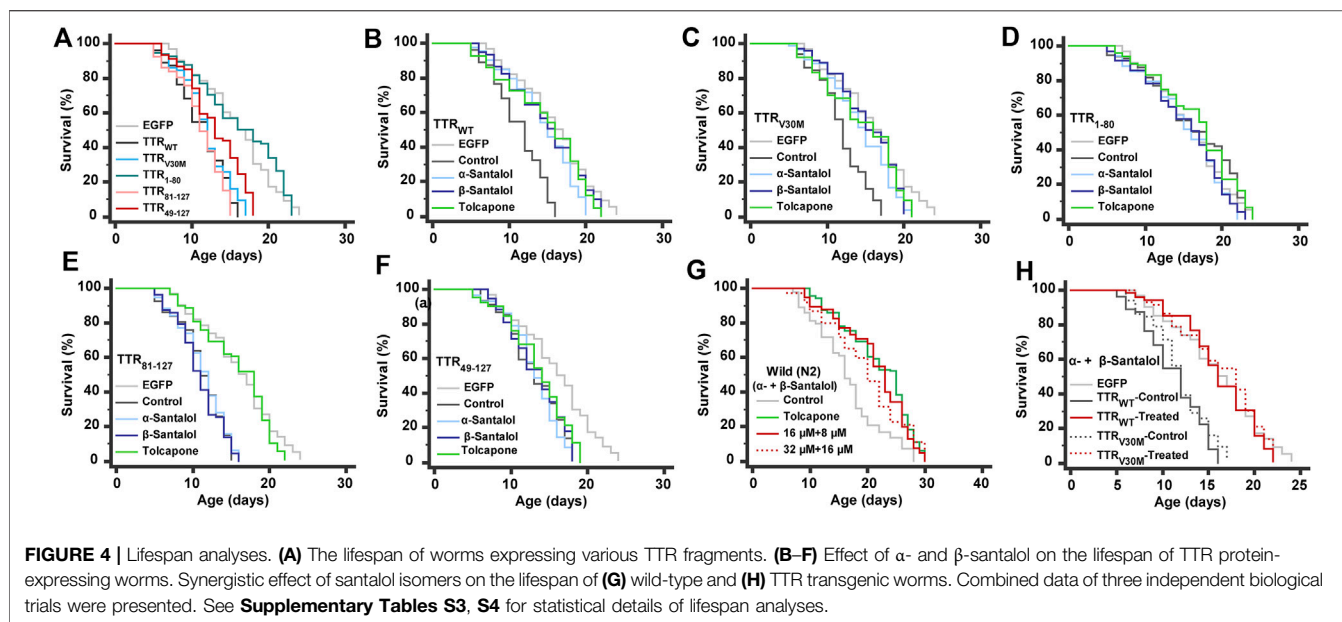
Data are presented as mean ± SD; ns-not significant, *p < 0.05, and **p < 0.01 vs. control.

clinically approved drugs for early-stage FAP, diflunisal and tafamidis (Sant'Anna et al., 2016). To measure the effect of these drug candidates on the formation of TTR aggregates, we counted the number of spherical shaped discrete structures in the transgenic worms grown in the presence or absence of α -santalol (32 μ M), β -santalol (16 μ M), and tolcapone (6 μ M) at 20°C. As shown in **Figure 3**, the results showed that supplementation of santalol isomers significantly inhibited the formation of TTR aggregates in worms expressing TTR_{WT}::EGFP and TTR_{V30M}::EGFP across various adulthood stages (day 2 and day 6). However, α - and β -santalol treatment exhibited a negligible effect on the aggregation of TTR₁₋₈₀::EGFP, TTR₈₁₋₁₂₇::EGFP, and TTR₄₉₋₁₂₇::EGFP when compared to that of untreated control. It was interesting to note that the TTR inhibitory potential of santalol isomers was found to be gradually increase as the worms aged. In earlier developmental stage (day 2 adulthood), α - and β -santalol treatment marginally decreased TTR_{WT} [21.6% ($p = 0.44$) and 19.8% ($p = 0.59$)] and TTR_{V30M} [16.8% ($p = 0.84$) and 29.1% ($p = 0.006$)] aggregates (**Supplementary Figure S2**). In addition, santalol isomers treatment was highly effective at inhibiting both TTR_{WT} [33.3% ($p < 0.01$) and 40.2% ($p < 0.01$)] and TTR_{V30M} [34.8% ($p < 0.01$) and 40.2%; ($p < 0.01$)] aggregation in day 6 adulthood worms. The effect of santalol isomers in preventing TTR aggregation was on par with the positive control tolcapone. Tolcapone treatment inhibits the aggregate formation in TTR_{WT}::EGFP [day 2–31.0% ($p = 0.06$), day 6–46.2% ($p < 0.01$)], TTR_{V30M}::EGFP [day 2–24.2% ($p = 0.21$), day 6–39.6% ($p < 0.01$)], and TTR₈₁₋₁₂₇::EGFP [day 2–30.3% ($p < 0.01$), day 6–48.0% ($p < 0.01$)] worms; however, it did not significantly affect TTR₁₋₈₀::EGFP, TTR₄₉₋₁₂₇::EGFP aggregates, but tolcapone treatment slightly reduce TTR formation ($p > 0.05$). We also explored the efficacy of combining α - and β -santalol on the aggregation of TTR in *C. elegans*. We systematically evaluated 12 possible combinations that can be formed out of four doses of α -santalol (4, 8, 16, and 32 μ M) and three doses of β -santalol (4, 8, and 16 μ M). It was observed that α -santalol combined with β -santalol, each at its half-optimal dose (16 and 8 μ M, respectively), lead to a significant reduction in the TTR_{WT}::EGFP [day 2–37.9% ($p = 0.37$); day 6–63.0% ($p < 0.01$)] and TTR_{V30M}::EGFP [day 2–36.5% ($p = 0.19$); day 6–52.5% ($p < 0.01$)] aggregates compared to the groups treated with single molecule and the control group. A few of the tested combinations also produced a noticeable impact on TTR aggregation, while their effect was not found to be synergistic than the half-optimal dose of santalol isomers, and some combinations showed no benefits (**Table 2**). These results indicated that the synergism between α - and β -santalol has the potential to inhibit the onset of TTR misfolding and aggregate formation in *C. elegans*.

α - and β -Santalol Extend the Lifespan of TTR Expressing *C. elegans*

Patients with TTR amyloidosis demonstrate several pathophysiological changes that ultimately lead to death within 10 years (Ando et al., 2005). Therefore, a small molecule with antiaging properties that can also improve TTR

degradation could be a viable strategy to treat FAP. We have previously shown that santalol isomers reduced the aggregation of toxic amyloid- β , α -synuclein, and polyglutamine proteins in *C. elegans*; these proteins are involved in the key pathological events in Alzheimer's, Parkinson's, and Huntington's diseases, respectively. In addition, santalol isomers extend the lifespan of *C. elegans* strains expressing these toxic proteins in body wall muscle cells and neurons (Mohankumar et al., 2018; Mohankumar et al., 2019b; Mohankumar et al., 2020). Taking into account the anti-aggregation and anti-aging potential of santalol isomers, we have tested their effects on the lifespan of worms expressing several TTR aggregates. Under standard laboratory conditions, the lifespan of worms expressing EGFP (control; 15.9 ± 0.4 days, $p = 0.39$) and TTR₁₋₈₀ (16.3 ± 0.5 days, $p = 0.23$) did not obviously alter compared to their wild-type counterparts (16.1 ± 0.5 days). However, worms expressing TTR_{WT} (29.3%, $p < 0.0001$), TTR_{V30M} (25.3%, $p < 0.0001$), TTR₈₁₋₁₂₇ (30.3%, $p < 0.0001$), and TTR₄₉₋₁₂₇ (17.8%, $p < 0.0001$) fragments had a significantly shorter lifespan (**Figure 4A**), suggest that these TTR fragments are likely proteotoxic, as is believed to be the case in humans. These findings are highly consistent with the previous reports (Madhivanan et al., 2018; Tsuda et al., 2018). We found that continuous exposure to α - and β -santalol treatment initiated during development (beginning from an embryo) led to lifespan extension in worms expressing TTR. After administering 32 μ M α -santalol, the mean lifespan of TTR_{WT} and TTR_{V30M} *C. elegans* increased to 14.4 ± 0.4 and 14.4 ± 0.3 days, respectively, which expanded the lifespan of worms by 27.6% ($p < 0.0001$) and 20.8% ($p < 0.0001$), respectively, compared to the control groups (**Figures 4B,C**). Similarly, β -santalol (16 μ M) treatment also significantly increased the mean lifespan of TTR_{WT} (**Figure 4B**) and TTR_{V30M} (**Figure 4C**) worms by 32.9% ($p < 0.0001$) and 27.8% ($p < 0.0001$), respectively. However, α - and β -santalol treatment would not further extend the lifespan of worms expressing TTR₁₋₈₀ ($p = 0.0958$; $p = 0.1264$) (**Figure 4D**), TTR₈₁₋₁₂₇ ($p = 0.5076$; $p = 0.5074$) (**Figure 4E**), and TTR₄₉₋₁₂₇ ($p = 0.3274$; $p = 0.6365$) (**Figure 4F**). We next investigated whether α -santalol and β -santalol can synergize to reduce the TTR toxicity and enhance the lifespan of TTR expressing *C. elegans*. To test this idea, initially we measured the lifespan of wild-type worms cultured on NGM plates carrying different concentrations of santalol isomers to identify the synergistic dose(s). Firstly, we observed that 16 μ M α -santalol and 8 μ M β -santalol together were the minimal dose to synergistically extend the lifespan of wild-type *C. elegans* by 28.0% under standard laboratory conditions (**Figure 4G**; **Supplementary Figure S3**). The combinatorial effect of santalol isomers is significantly higher (22.3%, $p < 0.01$) than the largest effect produced by each compound under similar conditions (Mohankumar et al., 2018; Mohankumar et al., 2020). Interestingly, the combination of α - and β -santalol at their optimal doses (32 and 16 μ M, respectively) is not synergistic and extends the mean lifespan of N2 worms by 19.0% (**Figure 4G**; **Supplementary Figure S3**). Secondly, we found that the dual combination of santalol isomers (16 μ M α -santalol+8 μ M β -santalol) consistently extended the mean lifespan of TTR_{WT} and



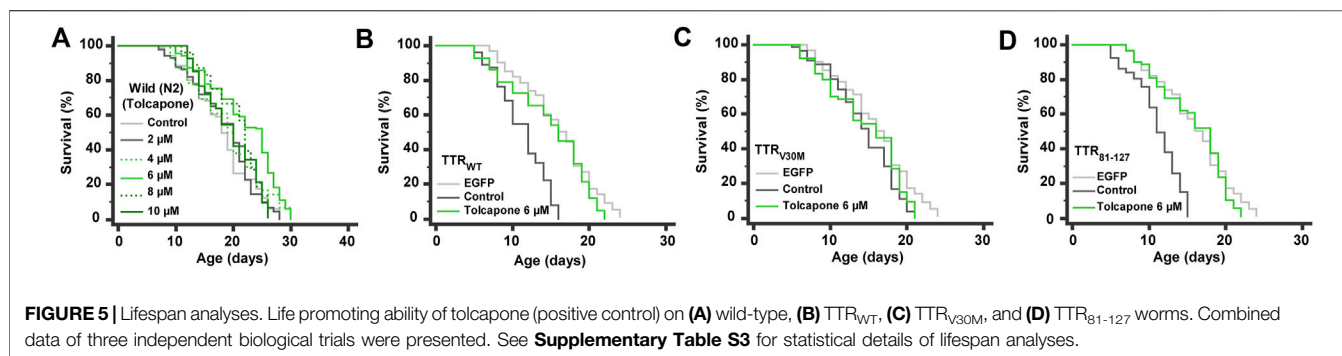
TTR_{V30M} expressing worms by 43.0 and 37.3%, while it did not obviously alter the lifespan of TTR_{1–80} ($p = 0.0826$), TTR_{81–127} ($p = 0.2477$), and TTR_{49–127} ($p = 0.2497$) worms (**Figure 4H**). In contrast to the dual combination, both α - and β -santalol were less effective separately on TTR worms. From this observation, it was apparent that a one-fold lower dose of santalol isomers together had a better pro-longevity effect on *C. elegans*; therefore, for the remainder of this study, we focused on the dual combination.

Surprisingly, we found that different pharmacological doses of tolcapone had different performances. Of the five concentrations, the survival curve of wild-type worms treated with 6 μ M tolcapone manifested not only a significant shift to the right but also had a mean lifespan of 21.9 ± 0.5 days (18.1 ± 0.5 days, untreated control) with a maximum lifespan of 30 days and increased by 21.2% in mean lifespan ($p < 0.0001$) (**Figure 5A**). Worms treated with 2 and 4 μ M tolcapone did not show a significant increase in mean lifespan, but their treatment marginally increased the mean lifespan by 2.3% ($p = 0.5247$) and 5.5% ($p = 0.0310$), respectively. Furthermore, worms cultured on 8 and 10 μ M tolcapone displayed a significantly different right-shifted survival curve when compared with unexposed control, and the mean lifespan was increased by 13.8 and 7.8%, respectively. Therefore, 6 μ M tolcapone was selected as the optimal concentration for most subsequent studies. On the other hand, tolcapone feeding increased the mean lifespan of TTR_{WT} (**Figure 5B**), TTR_{V30M} (**Figure 5C**), and TTR_{81–127} (**Figure 5D**) worms by 31.2% ($p < 0.0001$), 23.0% ($p < 0.0001$), and 41.7% ($p < 0.0001$) respectively, and it would not further extend the lifespan of TTR_{1–80} (3.3%, $p = 0.4205$) and TTR_{49–127} (4.0%, $p = 0.0906$) worms. Together these data imply that tolcapone can extend the lifespan of wild-type worms and worms expressing TTR at a relatively low dose; this may reduce or minimize the potential side effects (Olanow, 2000), which is relevant for future therapy against TTR amyloidosis. Our data provided the first insight into the life-promoting properties of

tolcapone, which will further promote it as an antiaging drug for a longer and healthier life for patients with TTR and related amyloidosis. However, the precise mechanism(s) underlying the longevity-promoting properties of tolcapone is still unexplored, and we are currently testing these possibilities.

Synergistic Inhibition of Transthyretin by Santalol Isomers Requires SKN-1/Nrf2, Autophagy, and Proteasome Functions

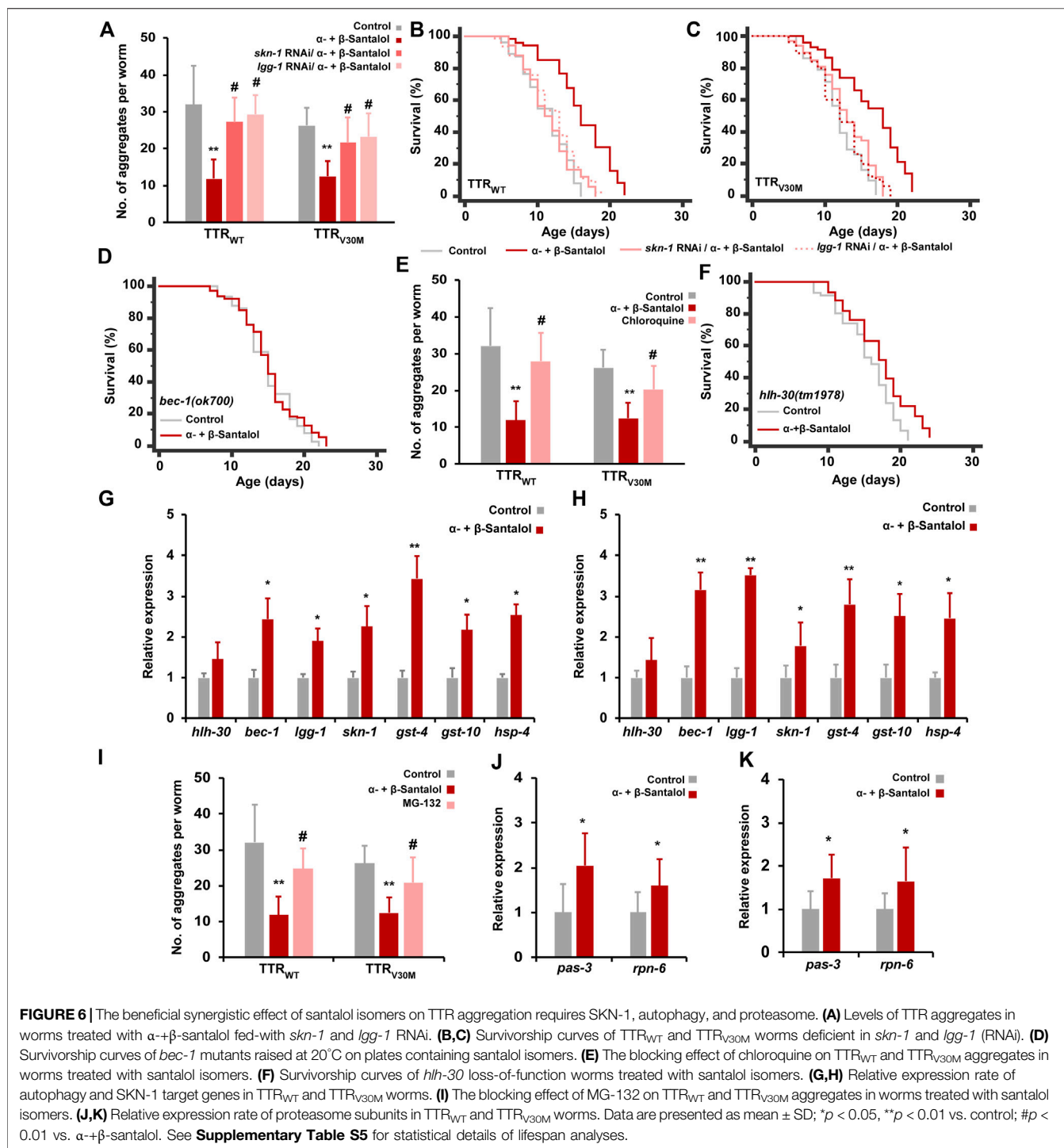
We next investigated the mechanism(s) by which the combination of α -+ β -santalol extends lifespan and inhibits TTR aggregation in *C. elegans*. In our previous study, we confirmed that α - and β -santalol selectively regulate the SKN-1/Nrf2 protective pathway to reduce oxidative (H_2O_2) (Mohankumar et al., 2019b), neurotoxic (6-OHDA) (Mohankumar et al., 2018), and proteotoxic (α -synuclein, β -amyloid, and polyQ) (Mohankumar et al., 2018; Mohankumar et al., 2020) stresses in *C. elegans*. It has been shown before that santalol isomers trigger the activation of autophagy in keratinocytes (Dickinson et al., 2014). Autophagy is a complex lysosome-dependent intracellular machinery that degrades misfolded and abnormal protein aggregates to maintain proteostasis. The accumulation of abnormal protein aggregates, a key pathological event in neurodegenerative diseases, can be reduced by autophagy. Dysregulated autophagic activity has been observed in most neurodegenerative diseases, which accelerates the disease progression (Nixon, 2013). Recent studies have shown that autophagy is impaired in experimental models and patients with TTR amyloidosis (Buxbaum, 2009). In *C. elegans*, autophagic activity has been reported to reduce TTR-mediated neurotoxicity and TTR oligomer and tetramer levels (Madhivanan et al., 2018). Extracellular deposition of mutant TTR fibril has also been shown to downregulate proteasome



functions (Santos et al., 2007). The proteasome is a multisubunit proteinase complex that is critical for the degradation of damaged and misfolded cellular proteins by the ubiquitin-proteasome system (UPS). Therefore, activating the SKN-1/Nrf2 protective pathway, autophagy, and the proteasome should be considered therapeutic targets for treating TTR amyloidosis. Having established that the combination of α - and β -santalol inhibits TTR aggregation and prolongs the lifespan of *C. elegans* expressing TTR fragments, we wondered if this effect was indeed due to the activation of SKN-1/Nrf2 and autophagic activity. First, we tested the requirement of SKN-1 in santalol isomers-mediated inhibition of TTR aggregation. Knockdown of *skn-1* using RNAi significantly blocked the reduction in TTR aggregation and prolongation of lifespan by α -+ β -santalol in TTR_{WT} ($p < 0.01$) and TTR_{V30M} ($p < 0.01$) worms (Figures 6A–C), suggesting the involvement of SKN-1. We next examined the role of autophagy in santalol isomers-induced reduction in TTR toxicity; therefore, we tested α -+ β -santalol effects in TTR_{WT}::EGFP and TTR_{V30M}::EGFP worms depleted of *lgg-1* (*lgg-1* RNAi) and *bec-1(ok700)* (mutant). *lgg-1* and *bec-1* are mammalian homologs of MAP-LC3 and Beclin1, respectively, and are required for the breakdown of cellular components by autophagy. It was observed that animals silenced with *lgg-1* RNAi were unresponsive to α -+ β -santalol treatment, since the number of TTR aggregates in TTR_{WT} ($p = 0.82$) and TTR_{V30M} ($p = 0.27$) worms were statistically similar to unexposed groups that received control RNAi or solvent (Figure 6A). *lgg-1* RNAi significantly reversed the longevity-promoting efficacy of α -+ β -santalol feeding in worms expressing wild-type (25.5%; $p < 0.0001$) (Figure 6B) and V30M mutant (25.1%; $p < 0.0001$) (Figure 6C) TTR. Furthermore, santalol isomers failed to extend the mean lifespan of worms bearing a loss of function mutation in the *bec-1* gene ($p = 0.3404$), identifying the underlying role of *bec-1* in santalol isomers-mediated TTR inhibition (Figure 6D). To further study the role of autophagy, we blocked the autophagic flux using chloroquine (10 mM). Chloroquine, a well-established antimalarial drug, has previously been shown to inhibit autophagic flux by reducing autophagosome-lysosome fusion and activity (Mauthe et al., 2018). The results showed that chloroquine treatment blocked the reduction in TTR_{WT} and TTR_{V30M} aggregation by α -+ β -santalol, so the worms treated with chloroquine/ α -+ β -santalol had almost the same aggregation pattern as unexposed worms ($p = 0.16$ and $p = 0.074$, respectively)

(Figure 6E). These results showed that autophagy is required for the synergistic effect of α -+ β -santalol on TTR aggregation.

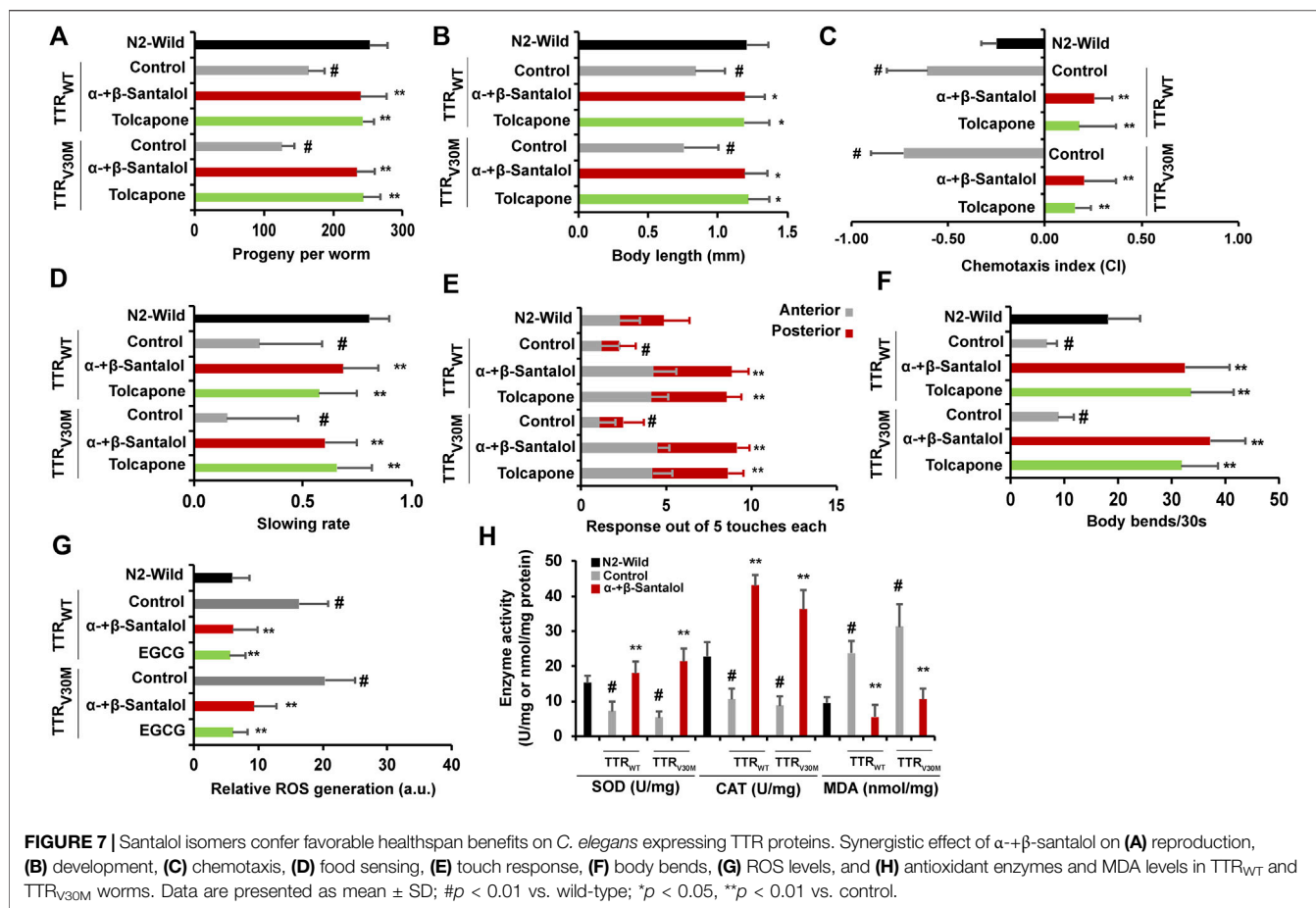
Given the dependency of autophagy in santalol isomers-mediated TTR inhibition, we tested the involvement of HLH-30 transcription factor. Recently, HLH-30, a mammalian helix-loop-helix transcription factor EB (TFEB), was shown to regulate longevity, stress resilience, and protein aggregation in *C. elegans*. In addition, HLH-30 regulates the expression of several genes involved in activating autophagy and lysosomal functions (Lapierre et al., 2013; Lin et al., 2018). α -+ β -Santalol treatment extended the lifespan of worms carrying the *hlh-30(tm 1978)* loss-of-function allele by 11.4% ($p < 0.0001$) (Figure 6F), but the increase was not the same as for wild-type N2 worms. We also noticed an increase in *hlh-30* mRNA levels in TTR_{WT} and TTR_{V30M} worms after treatment with α -+ β -santalol, but the increment was not statistically significant (Figures 6G,H). These results suggest that santalol isomers partially require the HLH-30 transcription factor to alleviate TTR-associated pathologies. To further validate the results, we measured the expression rate of SKN-1 direct target and autophagy genes in TTR_{WT} and TTR_{V30M} worms. α -+ β -Santalol treatment significantly upregulates the expression levels of autophagy genes *bec-1* and *lgg-1* and its direct transcriptional readouts including *gst-4*, *gst-10* (antioxidant genes), and *hsp-4* (ER chaperon) (Figures 6G,H). We also hypothesized that santalol isomers may have altered the proteasome system in worms expressing TTR fragments. To test the possibility, we first used the proteasome inhibitor MG-132 to block the proteasome functions and to check whether proteasome functions are necessary for the beneficial effect of santalol isomers on TTR aggregation in *C. elegans*. As shown in Figure 6I, 20 μ M MG-132 completely reversed the TTR aggregation inhibitory effect of α -+ β -santalol in TTR_{WT} and TTR_{V30M} worms. Thus, α -+ β -santalol inhibits the proteotoxicity and pathological symptoms of TTR by enhancing proteasome functions. We, therefore, evaluated the mRNA levels of various proteasome subunits (*pas-1-7*; *pbs-1-7*; *rpt-1-6*; *rpn-1-3*, and *rpn-5-12*) in TTR_{WT} and TTR_{V30M} worms treated with santalol isomers. After treatment with α -+ β -santalol, the transcript levels of *pas-3* and *rpn-5* were significantly upregulated ($p < 0.05$) (Figures 6J,K; Supplementary Figure S4). PAS-3 (20S proteasome subunit alpha type-4) is one of the critical components of the 20S proteasome and is involved



in the proteasomal protein catabolic process (wormbase.org). RPN-5 (proteasome 26S subunit, non-ATPase 12) is a conserved proteasome subunit required for proper proteasome localization and assembly (Yen et al., 2003). Altogether, these results suggested that santalol isomers exert their beneficial effects against TTR aggregation by activating the SKN-1/Nrf2 protective pathway, autophagy, and proteasome in *C. elegans*.

Santalol Isomers Improved the Physiological Functions of Transthyretin Expressing *C. elegans*

Interventions that inhibit the aggregation of toxic proteins and improve life expectancy do not necessarily increase health expectancy with age (Mohankumar et al., 2020). To test this idea, we examined the beneficial effects of α -+ β -santalol on a few



physiological parameters such as reproduction (progeny production), development (body length), chemotaxis, food sensing, motor activity (touch response and body bends), and antioxidant enzymes (superoxide dismutase [SOD] and catalase [CAT]) and malondialdehyde (MDA) levels in worms expressing TTR. First, we investigated the influence of santalol isomers on the reproduction and development of *C. elegans*. The results showed that expression of wild-type and V30M mutant TTR protein reduced progeny production and body length of *C. elegans*, while treatment with α - β -santalol significantly reversed natural reproduction and development (*p* < 0.01) (Figures 7A,B). Next, we studied the effects of santalol isomers on chemotaxis and food sensing behavior, and they have also been reported to decline with age in *C. elegans* (Mohankumar et al., 2020). In FAP patients, the deposition of TTR aggregates around autonomic and peripheral neurons is linked with the loss of nociception, a process that detects noxious stimuli (Coelho et al., 2013). Similarly, the expression of TTR_{V30M} in body wall muscle cells induces nonautonomous sensory nociception defects and affects dendritic outgrowth in *C. elegans* (Madhivanan et al., 2018). TTR_{WT} and TTR_{V30M} worms pre-exposed to α - β -santalol exhibit enhanced chemotaxis (Figure 7C) and food sensing behavior (Figure 7D) during the later adulthood stage (day 10; *p* < 0.01) compared to age-matched control worms, indicates the

healthy status of sensory neurons. Consistent with the previous observation, however, the expression of TTR_{WT} and TTR_{V30M} significantly reduced memory and learning ability in *C. elegans* (*p* < 0.01) than non-TTR control and wild-type animals, suggesting the neurotoxic property of TTR aggregates (Figures 7C,D; Madhivanan et al., 2018). To test whether santalol isomers protect the other neurons from TTR-induced toxicity, we evaluated soft-touch sensing ability. In *C. elegans*, the ability to sense and respond to touch is largely controlled by mechanoreceptor neurons and their functions decrease with age (Pan et al., 2011) and TTR aggregation (Madhivanan et al., 2018). We observed that day 10 adulthood wild-type worms exhibited a reduction in age-dependent anterior and posterior touch response, while TTR expression further reduced the response to soft touch. However, α - β -santalol treatment significantly improved the anterior and posterior touch response in worms expressing TTR_{WT} and TTR_{V30M} late in life (Figure 7E). To further investigate the effect of santalol isomers on motor activity, we compared the body bends (swimming vigor) between control and α - β -santalol treated groups in old age (day 10). As shown in Figure 7F, the swimming vigor of worms maintaining the expression of TTR_{WT} and TTR_{V30M} in body wall muscle cells was significantly lower than that of their wild-type counterparts. Besides, santalol isomers treated TTR_{WT} and TTR_{V30M} worms displayed enhanced

swimming vigor/body bends at old age than untreated controls. Interestingly, we found that the body bends of TTR expressing worms treated with α -+ β -santalol are remarkably higher than wild-type worms exposed to similar concentrations of santalol isomers.

Previously, the relationship between TTR levels and reactive oxygen species (ROS) in the tissues of patients with TTR deposits and *C. elegans* was established (Ando et al., 1997; Tsuda et al., 2018). Santalol isomers also reportedly possess antioxidant activity by quenching the free radicals (Mohankumar et al., 2018). Therefore, we measured the ROS levels in TTR expressing worms in the presence and absence of α -+ β -santalol using a ROS-specific fluorescent probe H₂DCF-DA. Results showed that the TTR_{WT} and TTR_{V30M} worms showed higher intracellular ROS levels. In the presence of α -+ β -santalol, however, the elevation in ROS levels observed in TTR_{WT} and TTR_{V30M} worms was significantly reduced to almost the control values (Figure 7G). We also examined the effect of santalol isomers on the activities of SOD, CAT, and MDA in TTR worms (Figure 7H). Day 5 adulthood worms expressing TTR_{WT} and TTR_{V30M} aggregates exhibited significantly reduced SOD and CAT activities compared to age-matched wild-type worms. Compared with the control, the SOD and CAT activities were restored and upregulated by α -+ β -santalol treatment. Furthermore, the levels of lipid peroxidation, as evidenced by MDA levels, were 76.8 and 66.4% lower in α -+ β -santalol-treated TTR_{WT} and TTR_{V30M} worms than those in untreated groups. Untreated worms from TTR_{WT} and TTR_{V30M} groups showed relatively higher levels of MDA compared to wild-type counterparts ($p < 0.01$), and the overproduction of MDA indicates oxidative damages (Figure 7H). These results clearly show that TTR aggregates generate intracellular ROS and that α -+ β -santalol exhibited antioxidant activity in *C. elegans*. From these observations, it was apparent that the synergism between α - and β -santalol improved several healthspan measures in *C. elegans* models of TTR amyloidosis during their early and late in life.

Conclusion

In summary, we have shown that santalol isomers are potent inhibitors of TTR amyloidogenesis. Santalol isomers effectively inhibit fibril formation and stabilize the native tetrameric form of TTR under denaturation conditions *in vitro*. We found that the combination of santalol isomers (α -+ β -santalol) acts synergistically to prevent TTR-induced toxicity, lifespan reduction, and other functional deficits in *C. elegans*. Moreover, santalol isomers interact with TTR variants (TTR_{WT} and TTR_{V30M}) and reduce the flexibility of the T₄ binding cavity and the homotetramer interface, which in turn confers the conformational stability of

TTR and prevents the dissociation of the tetramer and subsequent self-assembly into toxic aggregates. Santalol isomers inhibit TTR aggregation and help maintain proteostasis in *C. elegans* by activating the SKN-1/Nrf2 protective pathway, autophagy, and proteasome. SKN-1/Nrf2, autophagy, and proteasome are highly conserved between *C. elegans* and mammals, and hence it is not unfair to hypothesize that santalol isomers may also be protective against TTR-induced toxicity in patients with FAP, FAC, and/or SSA. Therefore, preclinical studies on mammalian models of TTR amyloidosis using a combination of santalol isomers are justified.

DATA AVAILABILITY STATEMENT

The raw data supporting the conclusions of this article will be made available by the authors, without undue reservation.

AUTHOR CONTRIBUTIONS

AM conducted all experiments, analyzed the results, and wrote the manuscript. DK and GT performed a few *in vivo* experiments and contributed to data analysis. SM, RS, and SV performed the molecular dynamics simulation and discussed the results. ST and PS conceptualized and supervised the project. All authors read and approved the final manuscript.

ACKNOWLEDGMENTS

This study was supported in part by Santalis Pharmaceuticals Inc. (San Antonio, TX, United States), who also provided some reagents used in the experiments. We thank Prof. Kunitoshi Yamanaka (Department of Molecular Cell Biology, Kumamoto University, Japan) for providing us with TTR *C. elegans* strains. Some strains were provided by the Caenorhabditis Genetic Centre (CGC, University of Minnesota, MN, United States), which is funded by the NIH Office of Research Infrastructure Programs (P40 OD010440). Special thanks go to Prof. Julie Ahringer (The Gurdon Institute, University of Cambridge, United Kingdom) for providing us with the RNAi clones.

SUPPLEMENTARY MATERIAL

The Supplementary Material for this article can be found online at: <https://www.frontiersin.org/articles/10.3389/fphar.2022.924862/full#supplementary-material>

REFERENCES

- Adams, D., Koike, H., Slama, M., and Coelho, T. (2019). Hereditary Transthyretin Amyloidosis: A Model of Medical Progress for a Fatal Disease. *Nat. Rev. Neurol.* 15, 387–404. doi:10.1038/s41582-019-0210-4
- Ando, Y., Nyhlin, N., Suhr, O., Holmgren, G., Uchida, K., el Sahly, M., et al. (1997). Oxidative Stress is Found in Amyloid Deposits in Systemic

Amyloidosis. *Biochem. Biophys. Res. Commun.* 232, 497–502. doi:10.1006/bbrc.1996.5997

- Ando, Y., Nakamura, M., and Araki, S. (2005). Transthyretin-related Familial Amyloidotic Polyneuropathy. *Arch. Neurol.* 62, 1057–1062. doi:10.1001/archneur.62.7.1057

- Benson, M. D., Buxbaum, J. N., Eisenberg, D. S., Merlini, G., Saraiva, M. J. M., Sekijima, Y., et al. (2020). Amyloid Nomenclature 2020: Update and Recommendations by the International Society of Amyloidosis (ISA)

- Nomenclature Committee. *Amyloid* 27, 217–222. doi:10.1080/13506129.2020.1835263
- Bergström, J., Gustavsson, A., Hellman, U., Sletten, K., Murphy, C. L., Weiss, D. T., et al. (2005). Amyloid Deposits in Transthyretin-Derived Amyloidosis: Cleaved Transthyretin is Associated with Distinct Amyloid Morphology. *J. Pathol.* 206, 224–232. doi:10.1002/path.1759
- Berk, J. L., Suhr, O. B., Obici, L., Sekijima, Y., Zeldenrust, S. R., Yamashita, T., et al. (2013). Repurposing Diflunisal for Familial Amyloid Polyneuropathy: A Randomized Clinical Trial. *JAMA* 310, 2658–2667. doi:10.1001/jama.2013.283815
- Brenner, S. (1974). The Genetics of *Caenorhabditis elegans*. *Genetics* 77, 71–94. doi:10.1093/genetics/77.1.71
- Bulawa, C. E., Connelly, S., DeVit, M., Wang, L., Weigel, C., Fleming, J. A., et al. (2012). Tafamidis, a Potent and Selective Transthyretin Kinetic Stabilizer that Inhibits the Amyloid Cascade. *Proc. Natl. Acad. Sci. U. S. A.* 109, 9629–9634. doi:10.1073/pnas.1121005109
- Buxbaum, J. N. (2009). Animal Models of Human Amyloidoses: Are Transgenic Mice Worth the Time and Trouble? *FEBS Lett.* 583, 2663–2673. doi:10.1016/j.febslet.2009.07.031
- Ciccione, L., Tonalì, N., Nencetti, S., and Orlandini, E. (2020). Natural Compounds as Inhibitors of Transthyretin Amyloidosis and Neuroprotective Agents: Analysis of Structural Data for Future Drug Design. *J. Enzyme Inhib. Med. Chem.* 35, 1145–1162. doi:10.1080/14756366.2020.1760262
- Coelho, T., Maurer, M. S., and Suhr, O. B. (2013). THAOS - The Transthyretin Amyloidosis Outcomes Survey: Initial Report on Clinical Manifestations in Patients with Hereditary and Wild-type Transthyretin Amyloidosis. *Curr. Med. Res. Opin.* 29, 63–76. doi:10.1185/03007995.2012.754348
- Devagi, G., Mohankumar, A., Shanmugam, G., Nivitha, S., Dallemer, F., Kalaivani, P., et al. (2018). Organoruthenium(II) Complexes Ameliorates Oxidative Stress and Impedes the Age Associated Deterioration in *Caenorhabditis elegans* through JNK-1/DAF-16 Signalling. *Sci. Rep.* 8, 7688. doi:10.1038/s41598-018-25984-7
- Dickinson, S. E., Olson, E. R., Levenson, C., Janda, J., Rusche, J. J., Alberts, D. S., et al. (2014). A Novel Chemopreventive Mechanism for a Traditional Medicine: East Indian Sandalwood Oil Induces Autophagy and Cell Death in Proliferating Keratinocytes. *Arch. Biochem. Biophys.* 558, 143–152. doi:10.1016/j.abb.2014.06.021
- Dong, M., Li, H., Hu, D., Zhao, W., Zhu, X., and Ai, H. (2016). Molecular Dynamics Study on the Inhibition Mechanisms of Drugs CQ 1–3 for Alzheimer Amyloid- β 40 Aggregation Induced by Cu²⁺. *ACS Chem. Neurosci.* 7, 599–614. doi:10.1021/acscchemneuro.5b00343
- Hammarström, P., Jiang, X., Hurshman, A. R., Powers, E. T., and Kelly, J. W. (2002). Sequence-dependent Denaturation Energetics: A Major Determinant in Amyloid Disease Diversity. *Proc. Natl. Acad. Sci. U. S. A.* 99, 16427–16432. doi:10.1073/pnas.202495199
- He, F. (2011). Total RNA Extraction From *C. elegans*. *Bio. Protocol.* 1 (6), e47. doi:10.21769/BioProtoc.47
- Hörnberg, A., Eneqvist, T., Olofsson, A., Lundgren, E., and Sauer-Eriksson, A. E. (2000). A Comparative Analysis of 23 Structures of the Amyloidogenic Protein Transthyretin. *J. Mol. Biol.* 302, 649–669. doi:10.1006/jmbi.2000.4078
- Holmgren, G., Steen, L., Ekstedt, J., Groth, C. G., Ericzon, B. G., Eriksson, S., et al. (1991). Biochemical Effect of Liver Transplantation in Two Swedish Patients with Familial Amyloidotic Polyneuropathy (FAP-Met30). *Clin. Genet.* 40, 242–246. doi:10.1111/j.1399-0004.1991.tb03085.x
- Huber, P., Flynn, A., Sultan, M. B., Li, H., Rill, D., Ebede, B., et al. (2019). A Comprehensive Safety Profile of Tafamidis in Patients with Transthyretin Amyloid Polyneuropathy. *Amyloid* 26, 203–209. doi:10.1080/13506129.2019.1643714
- Hurshman, A. R., White, J. T., Powers, E. T., and Kelly, J. W. (2004). Transthyretin Aggregation under Partially Denaturing Conditions Is a Downhill Polymerization. *Biochemistry* 43, 7365–7381. doi:10.1021/bi049621i
- Johnson, S. M., Wiseman, R. L., Sekijima, Y., Green, N. S., Adamski-Werner, S. L., and Kelly, J. W. (2005). Native State Kinetic Stabilization as a Strategy to Ameliorate Protein Misfolding Diseases: A Focus on the Transthyretin Amyloidosis. *Acc. Chem. Res.* 38, 911–921. doi:10.1021/ar020073i
- Klabunde, T., Petrassi, H. M., Oza, V. B., Raman, P., Kelly, J. W., and Sacchettini, J. C. (2000). Rational Design of Potent Human Transthyretin Amyloid Disease Inhibitors. *Nat. Struct. Biol.* 7, 312–321. doi:10.1038/74082
- Lapierre, L. R., De Magalhães Filho, C. D., McQuary, P. R., Chu, C. C., Visvikis, O., Chang, J. T., et al. (2013). The TFEB Orthologue HLH-30 Regulates Autophagy and Modulates Longevity in *Caenorhabditis elegans*. *Nat. Commun.* 4, 2267. doi:10.1038/ncomms3267
- Lin, X. X., Sen, I., Janssens, G. E., Zhou, X., Fonslow, B. R., Edgar, D., et al. (2018). DAF-16/FOXO and HLH-30/TFEB Function as Combinatorial Transcription Factors to Promote Stress Resistance and Longevity. *Nat. Commun.* 9, 4400. doi:10.1038/s41467-018-06624-0
- Lozeron, P., Théaudin, M., Mincheva, Z., Ducot, B., Lacroix, C., and Adams, D. (2013). Effect on Disability and Safety of Tafamidis in Late Onset of Met30 Transthyretin Familial Amyloid Polyneuropathy. *Eur. J. Neurol.* 20, 1539–1545. doi:10.1111/ene.12225
- Madhivanan, K., Greiner, E. R., Alves-Ferreira, M., Soriano-Castell, D., Rouzbeh, N., Aguirre, C. A., et al. (2018). Cellular Clearance of Circulating Transthyretin Decreases Cell-Nonautonomous Proteotoxicity in *Caenorhabditis elegans*. *Proc. Natl. Acad. Sci. U. S. A.* 115, E7710–E7719. doi:10.1073/pnas.1801117115
- Matsushita, H., Isoguchi, A., Okada, M., Masuda, T., Misumi, Y., Tsutsui, C., et al. (2021). Glavonoid, a Possible Supplement for Prevention of ATTR Amyloidosis. *Heliyon* 7, e08101. doi:10.1016/j.heliyon.2021.e08101
- Mauthe, M., Orhon, I., Rocchi, C., Zhou, X., Luhr, M., Hijlkema, K. J., et al. (2018). Chloroquine Inhibits Autophagic Flux by Decreasing Autophagosome-Lysosome Fusion. *Autophagy* 14, 1435–1455. doi:10.1080/15548627.2018.1474314
- Mohankumar, A., Shanmugam, G., Kalaiselvi, D., Levenson, C., Nivitha, S., Thiruppathi, G., et al. (2018). East Indian Sandalwood (Santalum album L.) Oil Confers Neuroprotection and Geroprotection in *Caenorhabditis elegans* via Activating SKN-1/Nrf2 Signaling Pathway. *RSC Adv.* 8, 33753–33774. doi:10.1039/C8RA05195J
- Mohankumar, A., Devagi, G., Shanmugam, G., Nivitha, S., Sundararaj, P., Dallemer, F., et al. (2019a). Organoruthenium(II) Complexes Attenuate Stress in *Caenorhabditis elegans* through Regulating Antioxidant Machinery. *Eur. J. Med. Chem.* 168, 123–133. doi:10.1016/j.ejmech.2019.02.029
- Mohankumar, A., Kalaiselvi, D., Levenson, C., Shanmugam, G., Thiruppathi, G., Nivitha, S., et al. (2019b). Antioxidant and Stress Modulatory Efficacy of Essential Oil Extracted from Plantation-Grown Santalum Album L. *Industrial Crops Prod.* 140, 111623. doi:10.1016/j.indcrop.2019.111623
- Mohankumar, A., Kalaiselvi, D., Thiruppathi, G., Muthusaravanan, S., Nivitha, S., Levenson, C., et al. (2020). α - and β -Santalols Delay Aging in *Caenorhabditis elegans* via Preventing Oxidative Stress and Protein Aggregation. *ACS Omega* 5, 32641–32654. doi:10.1021/acsomega.0c05006
- Nixon, R. A. (2013). The Role of Autophagy in Neurodegenerative Disease. *Nat. Med.* 19, 983–997. doi:10.1038/nm.3232
- Olanow, C. W. (2000). Tolcapone and Hepatotoxic Effects. Tasmarr Advisory Panel. *Arch. Neurol.* 57, 263–267. doi:10.1001/archneur.57.2.263
- Pan, C. L., Peng, C. Y., Chen, C. H., and McIntire, S. (2011). Genetic Analysis of Age-dependent Defects of the *Caenorhabditis elegans* Touch Receptor Neurons. *Proc. Natl. Acad. Sci. U. S. A.* 108, 9274–9279. doi:10.1073/pnas.1011711108
- Patil, R., Das, S., Stanley, A., Yadav, L., Sudhakar, A., and Varma, A. K. (2010). Optimized Hydrophobic Interactions and Hydrogen Bonding at the Target-Ligand Interface Leads the Pathways of Drug-Designing. *PLoS One* 5, e12029. doi:10.1371/journal.pone.0012029
- Pinney, J. H., Whelan, C. J., Petrie, A., Dungu, J., Banypersad, S. M., Sattianayagam, P., et al. (2013). Senile Systemic Amyloidosis: Clinical Features at Presentation and Outcome. *J. Am. Heart Assoc.* 2, e000098. doi:10.1161/JAHA.113.000098
- Rowczenio, D. M., Noor, I., Gillmore, J. D., Lachmann, H. J., Whelan, C., Hawkins, P. N., et al. (2014). Online Registry for Mutations in Hereditary Amyloidosis Including Nomenclature Recommendations. *Hum. Mutat.* 35, E2403–E2412. doi:10.1002/humu.22619
- Saelices, L., Johnson, L. M., Liang, W. Y., Sawaya, M. R., Cascio, D., Ruchala, P., et al. (2015). Uncovering the Mechanism of Aggregation of Human Transthyretin. *J. Biol. Chem.* 290, 28932–28943. doi:10.1074/jbc.M115.659912
- Sant'Anna, R., Gallego, P., Robinson, L. Z., Pereira-Henriques, A., Ferreira, N., Pinheiro, F., et al. (2016). Repositioning Tolcapone as a Potent Inhibitor of Transthyretin Amyloidogenesis and Associated Cellular Toxicity. *Nat. Commun.* 7, 10787. doi:10.1038/ncomms10787
- Santos, S. D., Cardoso, I., Magalhães, J., and Saraiva, M. J. (2007). Impairment of the Ubiquitin-Proteasome System Associated with Extracellular Transthyretin Aggregates in Familial Amyloidotic Polyneuropathy. *J. Pathol.* 213, 200–209. doi:10.1002/path.2224

- Sivaramakrishnan, M., Sharavanan, V. J., Durairaj, D. R., Kandaswamy, K., Piramanayagam, S., and Kothandan, R. (2019). Screening of Curcumin Analogues Targeting Sortase A Enzyme of *Enterococcus faecalis*: A Molecular Dynamics Approach. *J. Proteins Proteom* 10, 245–255. doi:10.1007/s42485-019-00020-y
- Stiernagle, T. (2006). Maintenance of *C. elegans*. *WormBook*. doi:10.1895/wormbook.1.101.1
- Tian, W., Chen, C., Lei, X., Zhao, J., and Liang, J. (2018). CASTp 3.0: Computed Atlas of Surface Topography of Proteins. *Nucleic Acids Res.* 46, W363–W367. doi:10.1093/nar/gky473
- Timmons, L., Court, D. L., and Fire, A. (2001). Ingestion of Bacterially Expressed dsRNAs Can Produce Specific and Potent Genetic Interference in *Caenorhabditis elegans*. *Gene* 263, 103–112. doi:10.1016/S0378-1119(00)00579-5
- Trott, O., and Olson, A. J. (2009). AutoDock Vina: Improving the Speed and Accuracy of Docking With a New Scoring Function, Efficient Optimization, and Multithreading. *J. Comput. Chem* 31 (2), 455–461. doi:10.1002/jcc.21334
- Tsuda, Y., Yamanaka, K., Toyoshima, R., Ueda, M., Masuda, T., Misumi, Y., et al. (2018). Development of Transgenic *Caenorhabditis elegans* Expressing Human Transthyretin as a Model for Drug Screening. *Sci. Rep.* 8, 17884. doi:10.1038/s41598-018-36357-5
- Yen, H. C., Espiritu, C., and Chang, E. C. (2003). Rpn5 is a Conserved Proteasome Subunit and Required for Proper Proteasome Localization and Assembly. *J. Biol. Chem.* 278, 30669–30676. doi:10.1074/jbc.M302093200
- Yokoyama, T., and Mizuguchi, M. (2020). Transthyretin Amyloidogenesis Inhibitors: From Discovery to Current Developments. *J. Med. Chem.* 63, 14228–14242. doi:10.1021/acs.jmedchem.0c00934

Conflict of Interest: The authors declare that the research was conducted in the absence of any commercial or financial relationships that could be construed as a potential conflict of interest.

Publisher's Note: All claims expressed in this article are solely those of the authors and do not necessarily represent those of their affiliated organizations, or those of the publisher, the editors and the reviewers. Any product that may be evaluated in this article, or claim that may be made by its manufacturer, is not guaranteed or endorsed by the publisher.

Copyright © 2022 Mohankumar, Kalaiselvi, Thirupathi, Muthusaravanan, Vijayakumar, Suresh, Tawata and Sundararaj. This is an open-access article distributed under the terms of the Creative Commons Attribution License (CC BY). The use, distribution or reproduction in other forums is permitted, provided the original author(s) and the copyright owner(s) are credited and that the original publication in this journal is cited, in accordance with accepted academic practice. No use, distribution or reproduction is permitted which does not comply with these terms.